Electronic Supplementary Information (ESI) for

Universal Passive Radiative Cooling Behavior of Aerogels

Bingjie Ma[a,b], Bing Wu[c], Peiying Hu[a], Ling Liu[a,b], Jin Wang[a,b,]*

[a] Key Laboratory of Multifunctional Nanomaterials and Smart Systems, Suzhou Institute of Nano-Tech and Nano-Bionics, Chinese Academy of Sciences, Suzhou 215123, P. R. China

[b] School of Nano-Tech and Nano-Bionics, University of Science and Technology of China, Hefei 230026, P. R. China

[c] Emergency Research Institute, Chinese Institute of Coal Science, Beijing 100013, P. R. China.

*E-mail: jwang2014@sinano.ac.cn

Supplementary Figures:

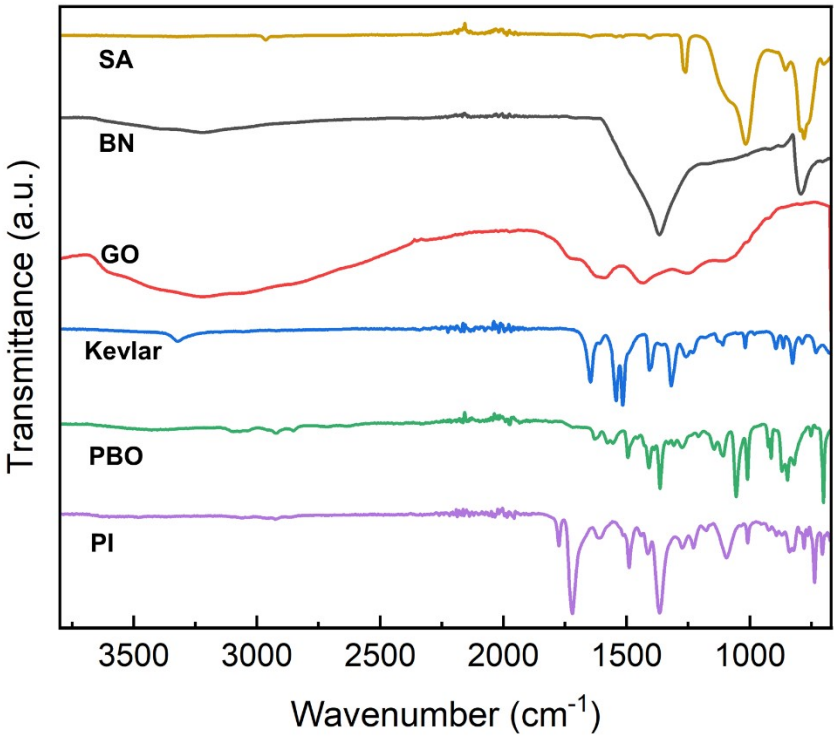

Fig. S1. TF-IR spectra of the aerogels.

Fig. S1 shows the FT-IR spectra of the silica, BN, GO, Kevlar, PBO, and PI aerogels. For the silica aerogel, the vibration peaks at 2980 cm^{-1} can be clearly observed, corresponding to that of $-CH_3$. Besides, the vibration peaks of Si-O-Si and Si-C can be observed at 1100 and 840 cm^{-1}, respectively. For the NB aerogels, there are two strong characteristic absorptions at 1350 cm^{-1} and 796 cm^{-1}, which are owing to the B–N stretching vibration and B–N out-of-plane vibration bending, respectively. For GO aerogels, the two peaks at 1739 and 1590 cm^{-1} could be attributed to the stretching vibrations of C=O and C=C on GO. For Kevlar aerogel, the main organic functional groups, 3321(N-H), 1644 (C=O), and 1017 cm^{-1} (C-H) can be observed. In PBO aerogel, oxazole ring deformation at 848 cm^{-1}, C-O bond stretch at 925 cm^{-1}, benzene ring deformation at 1010 cm^{-1}, C-N bond stretch at 1366 cm^{-1}, C-O, C-C, and oxazole ring deformation abbreviation at 1496 cm^{-1}, can be identified. For PI aerogels, the peak at 1366 cm^{-1} is assigned to the vibration of the imide ring (C-N), and the peak at 1719 cm^{-1} is attributed to the imide linkage.

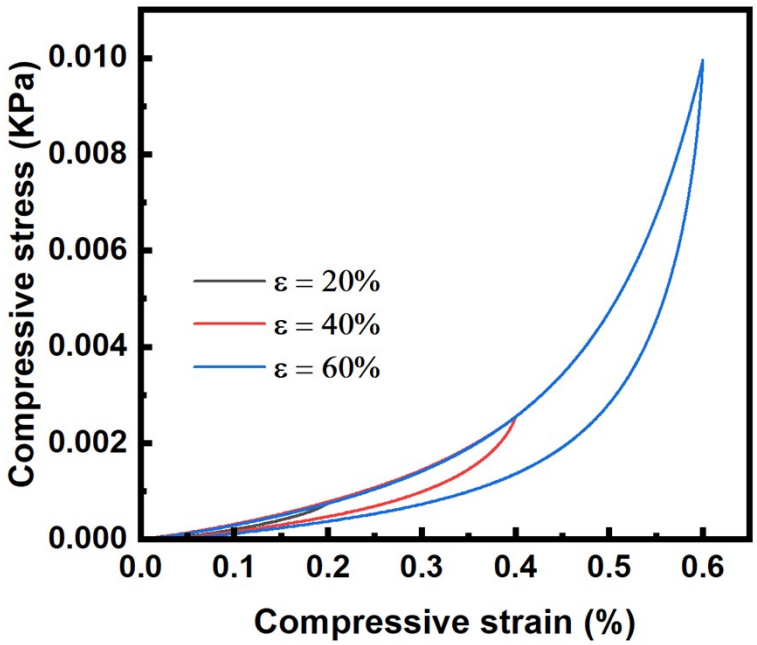

Fig. S2. The compression σ-ε curve of the silica aerogel loading - unloading period with increasing ε and the experimental snapshot of the period, ε is 20, 40, and 60 %, respectively.

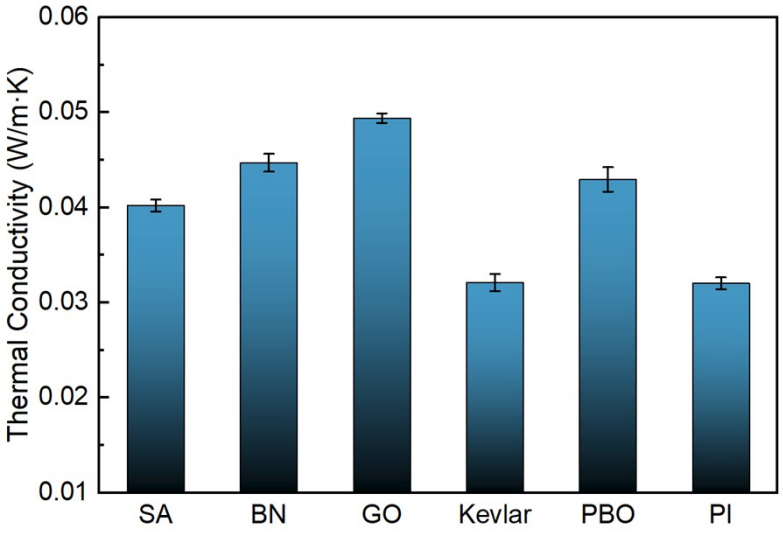

Fig. S3. Thermal conductivities of the aerogels.

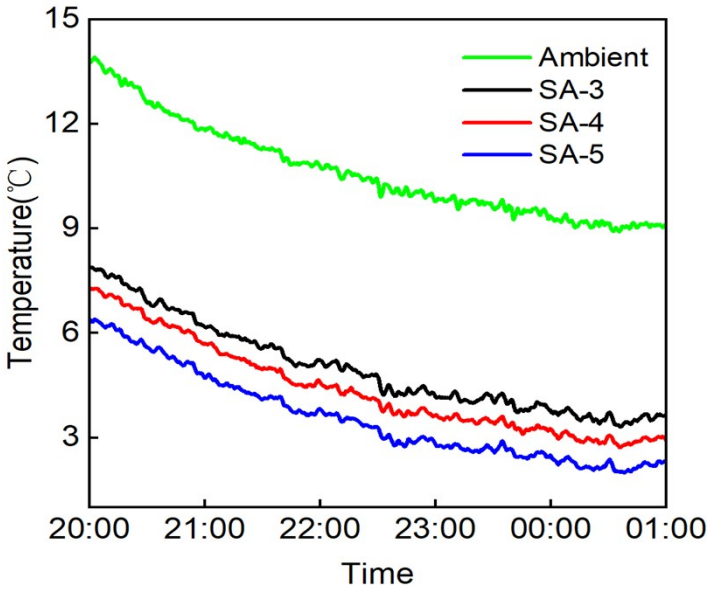

Fig. S4. The PRC performance of the SA with different thicknesses as indicated

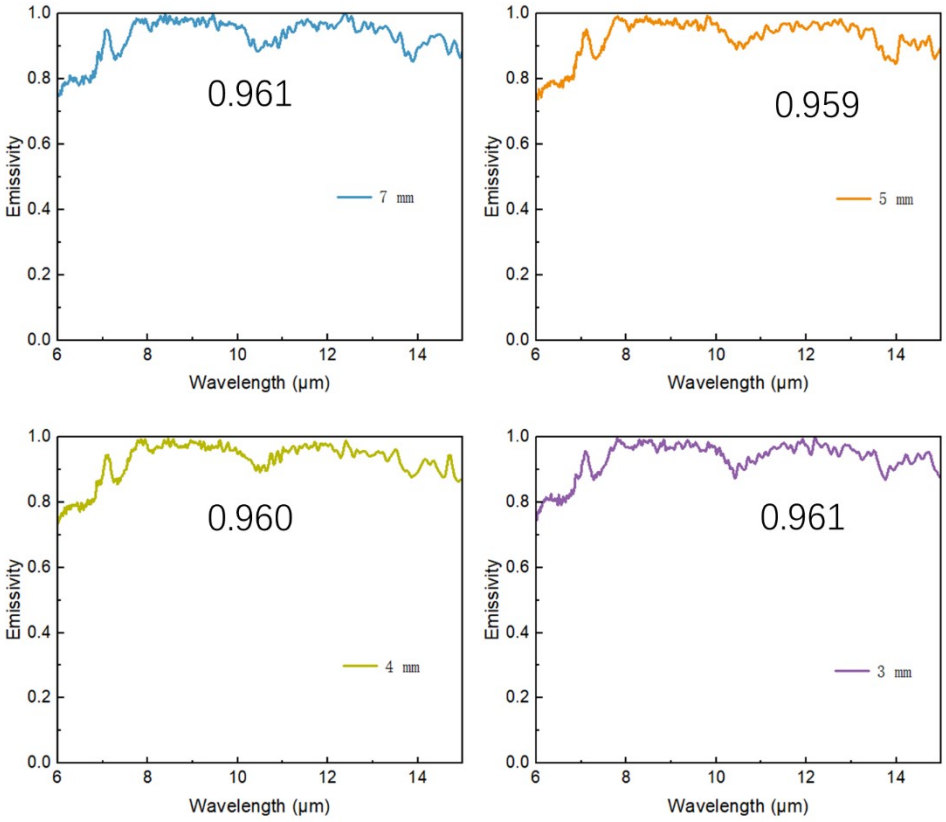

Fig. S5. The IR emissivity of the SA with different thicknesses as indicated.

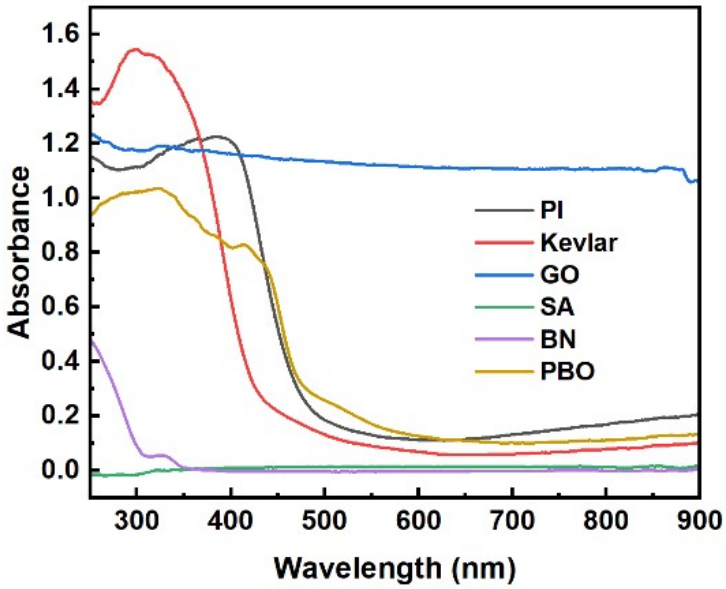

Fig. S6. Infrared absorption of each aerogel in the UV-Vis-NIR band.